Electronic Supplementary Material (ESI) for Journal of Materials Chemistry C.

Bismuth Triiodide Complexes: Structure, Spectroscopy, Electronic Properties, and Memristive Properties

Ewelina Wlaźlak,*[a] Justyna Kalinowska-Tłuścik,[b] Dawid Przyczyna,[ac] Piotr Zawal,[ac] and Konrad Szaciłowski*[a]

[a]AGH University of Science and Technology, Academic Centre for Materials and Nanotechnology, al. A. Mickiewicza 30, 30-059 Kraków, Poland.

[b]Faculty of Chemistry, Jagiellonian University, ul. Gronostajowa 2, 30-060 Kraków, Poland.

[c]Faculty of Physics and Applied Computer Science AGH University of Science and Technology al. A. Mickiewicza 30, 30-059 Kraków, Poland.

*corresponding authors

Content

Crystallographic details

Table S1. Crystal/experimental data and structure refinement results

Empirical moiety formula	$[BiI_3\{(C_6H_5)_3PO\}_2]$	$[BiI_3(C_5H_5NO)]$	$[BiI_3\{(C_6H_5)_2SO\}_{1.5}]_2$	$[BiI_3(C_{12}H_8N_2O_2)]$
Formula weight [g/mol]	1146.22	684.78	1786.14	801.88
Crystal system	Monoclinic	Triclinic	Triclinic	Triclinic
Space group	$P2_1/c$	$P\bar{1}$	$P\bar{1}$	$P\bar{1}$
Unite cell dimensions	a = 12.7693(3) Å b = 11.7066(1) Å c = 30.5274(7) Å a= 90.0° b= 127.090(3)° g= 90.0°	a = 7.6306(7) Å b = 8.6042 (9)Å c = 9.2988(9) Å a= 80.893(8)° b= 86.043(8)° g= 80.695(8)°	a = 11.2571(4)Å b = 13.8388(5)Å c = 16.8099(7)Å a= 82.885(3)° b= 77.008(3)° g= 67.450(4)°	a = 7.6873(3)Å b = 9.9765(4)Å c = 11.2378(4)Å a= 104.186(4)° b= 93.222(3)° g= 99.194(4)°
Volume [$Å^3$]	3640.17(17)	594.30(10)	2354.54(17)	820.73(6)
Z	4	2	2	2
D_{calc} [Mg/m^3]	2.091	3.827	2.519	3.245
μ [mm^{-1}]	7.506	22.582	11.561	16.385
F(000)	2136	584	1604	704
Crystal size [mm^3]	0.3 x 0.2 x 0.2	0.2 x 0.1 x 0.1	0.1 x 0.08 x 0.08	0.1 x 0.1 x 0.1
Θ range	3.05° to 28.57°	3.04° to 28.45°	2.98° to 28.57°	3.13° to 28.65°
Index ranges	-15 ≤ h ≤ 17, -15 ≤ k ≤ 14, -40 ≤ l ≤ 39	-7 ≤ h ≤ 10, -10 ≤ k ≤ 11, -12 ≤ l ≤ 12	-14 ≤ h ≤ 15, -18 ≤ k ≤ 17, -22 ≤ l ≤ 21	-10 ≤ h ≤ 9, -12 ≤ k ≤ 13, -15 ≤ l ≤ 14
Refl. collected	48661	4361	32076	10984
Independent reflections	8712 [R(int) = 0.1173]	2659 [R(int) = 0.0721]	10795 [R(int) = 0.0713]	3820 [R(int) = 0.0501]
Completeness [%] to Θ = 25.24°	99.8	99.8	99.8	99.9
Absorption correction	Analytical *)	Analytical	Analytical	Multi-scan
Tmin. and Tmax.	0. 073 and 0.295	0.178 and 0.644	0.384 and 0.605	0.859 and 1.000
Data/ restraints/parameters	8712 / 0 / 397	2659 / 0 / 70	10795 / 0 / 433	3820 / 0 / 181
GooF on F2	1.048	1.089	1.035	1.019
Final R indices [I>2sigma(I)]	R1= 0.0464, wR2= 0.1015	R1= 0.0629, wR2= 0.1157	R1= 0.0464, wR2= 0.0598	R1= 0.0268, wR2= 0.0493
R indices (all data)	R1= 0.0544, wR2= 0.1099	R1= 0.0969, wR2= 0.1417	R1= 0.0903, wR2= 0.0738	R1= 0.0333, wR2= 0.0520
$\Delta\rho_{max}$, $\Delta\rho_{min}$ [$e \cdot Å^{-3}$]	3.20 and -2.57	3.56 and -3.77	2.54 and -1.36	0.99 and -1.61

*) CrysAlisPro 1.171.40.14e (Rigaku Oxford Diffraction, 2018); Analytical numeric absorption correction using a multifaceted crystal model based on expressions derived by R.C. Clark & J.S. (Clark, R. C. & Reid, J. S. (1995). Acta Cryst. A51, 887-897)

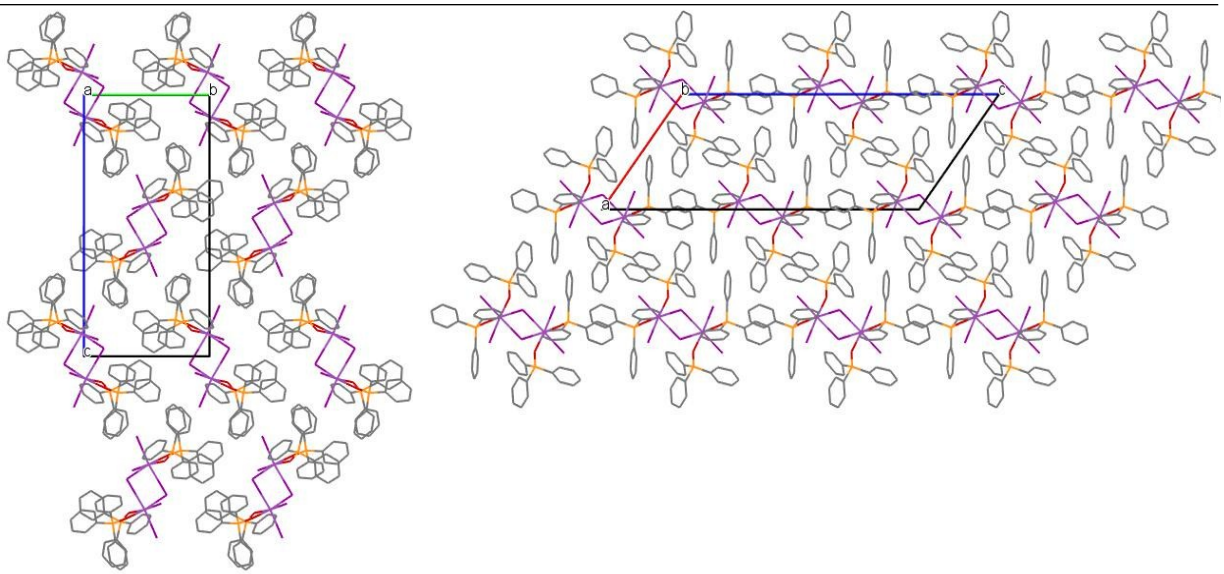

View along [100] View along [010]

Figure S1. Packing in the crystal of [BiI3{(C6H5)3PO}2]2 showing isolated centrosymmetric dimers. Hydrogen atoms were omitted for figure clarity.

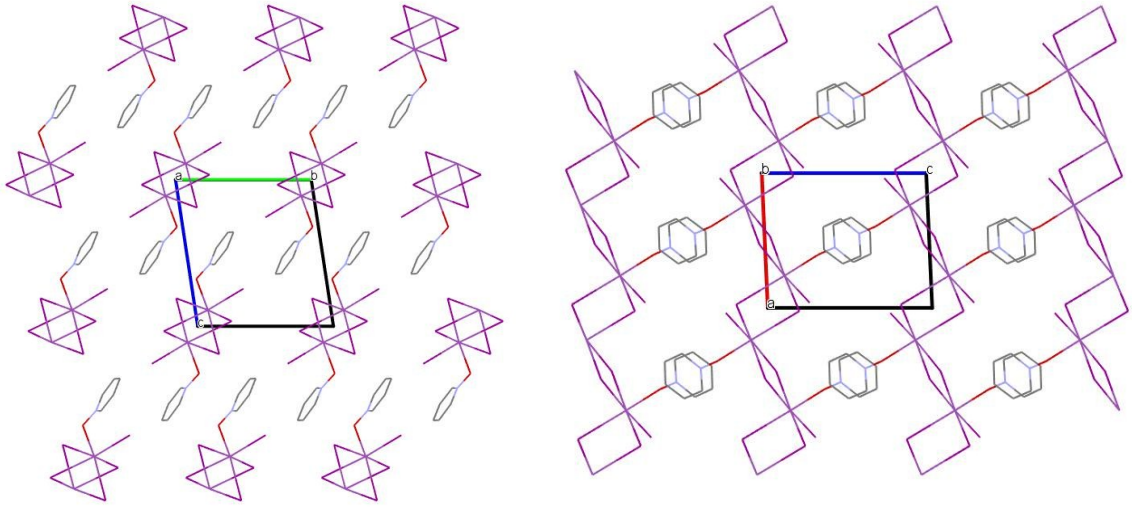

View along [100] View along [010]

Figure S2. Packing in the crystal of $[BiI_3(C_5H_5NO)]_n$ showing bismuth-iodide chains propagating parallel to [100] axis. Hydrogen atoms were omitted for figure clarity.

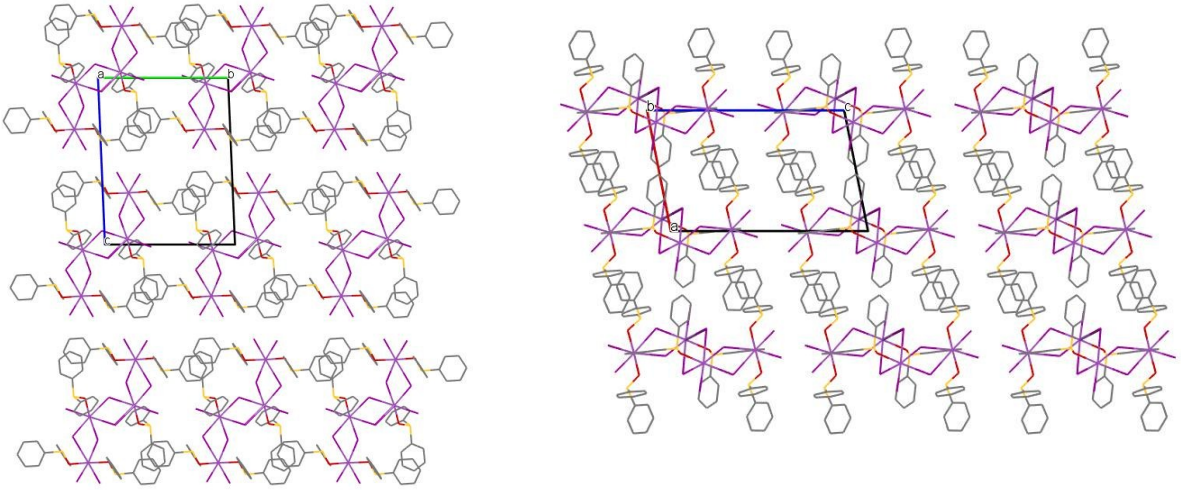

View along [100] View along [010]

Figure S3. Packing in the crystal of $[BiI_3\{(C_6H_5)_2SO\}_{1.5}]_4$ showing the isolated motives formed by 4 bismuth ions, bridged by iodide. Hydrogen atoms were omitted for figure clarity.

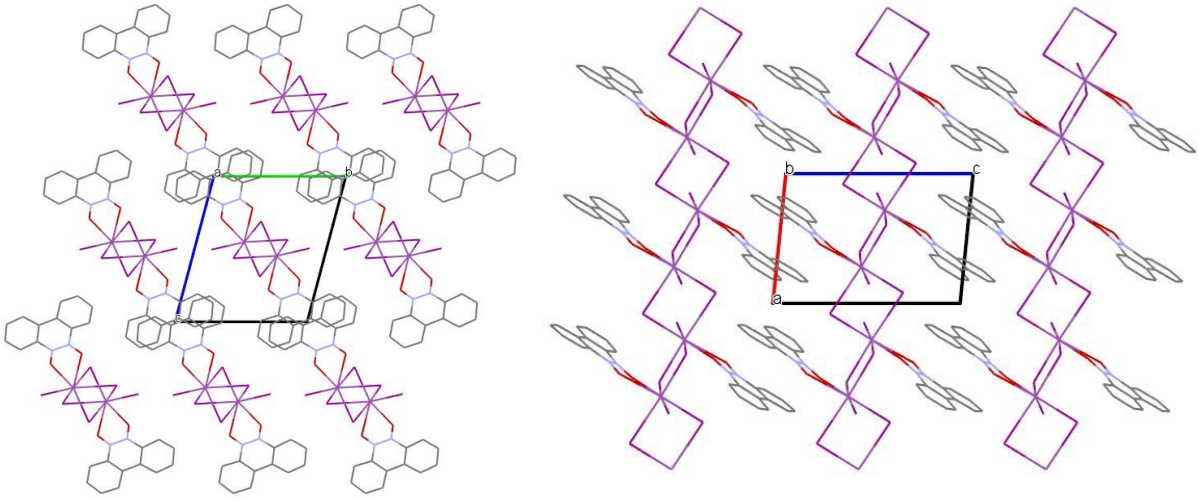

View along [100] View along [010]

Figure S4. Packing in the crystal of $[BiI_3(C_{12}H_8N_2O_2)]_n$ showing bismuth-iodide chains propagating parallel to [100] axis. Hydrogen atoms were omitted for figure clarity.

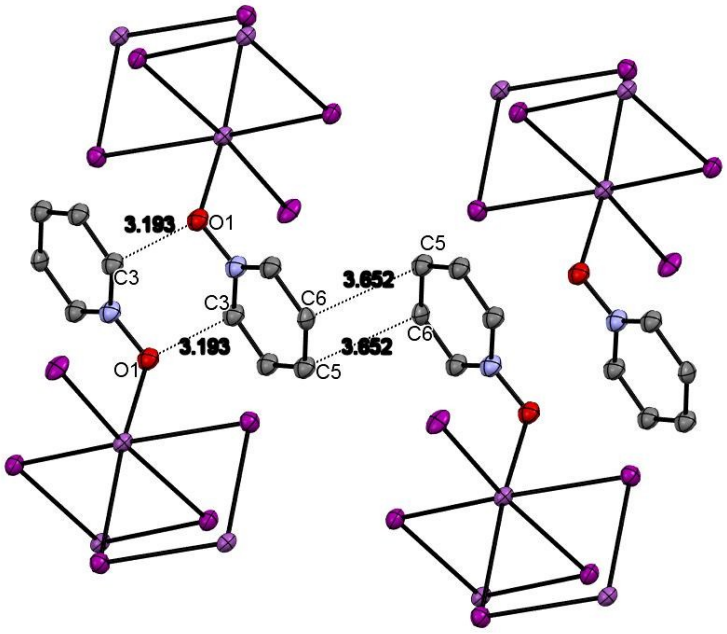

Figure S5. C...O short contacts between aromatic moieties in the crystal of $[BiI_3(C_5H_5NO)]_n$. Hydrogen atoms were omitted for figure clarity.

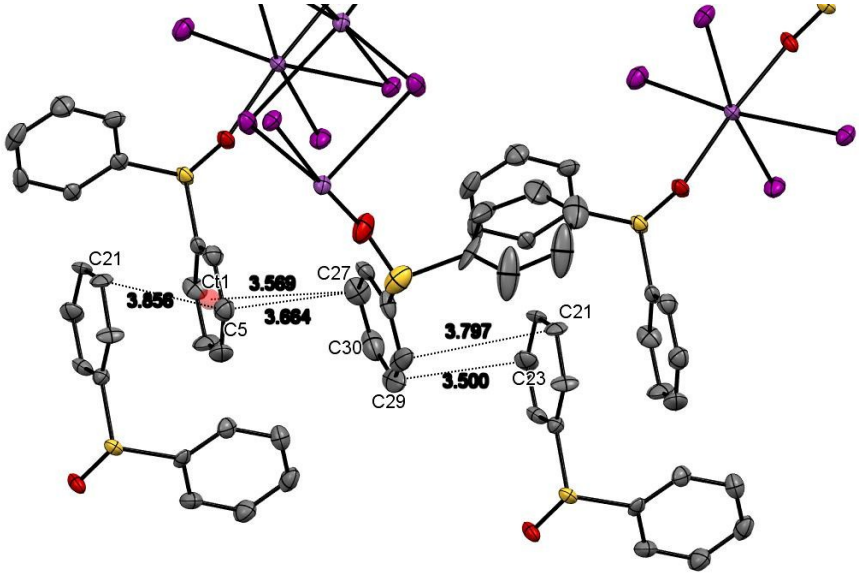

Figure S6. Short contacts between aromatic moieties (ring C1-C6, with shown Ct1 centre of gravity) in the crystal of $[BiI_3\{(C_6H_5)_2SO\}_{1.5}]_4$. Hydrogen atoms were omitted for figure clarity.

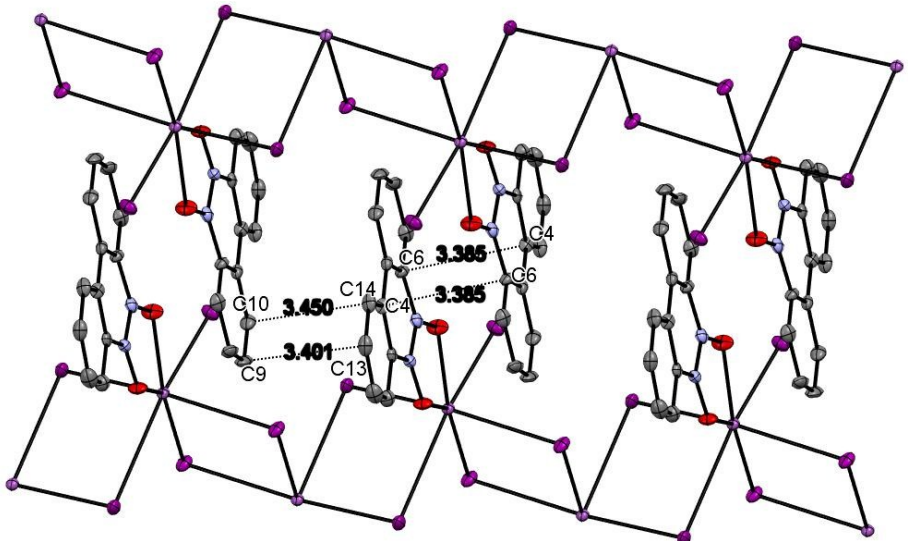

Figure S7. Short contacts and π...π interactions between aromatic moieties in the crystal of $[BiI_3(C_{12}H_8N_2O_2)]_n$. Hydrogen atoms were omitted for figure clarity.

Tauc plots and band gaps

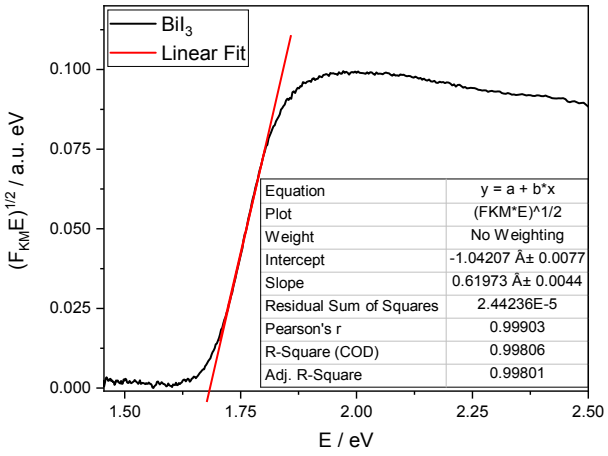

Figure S8. Tauc plots for BiI_3.

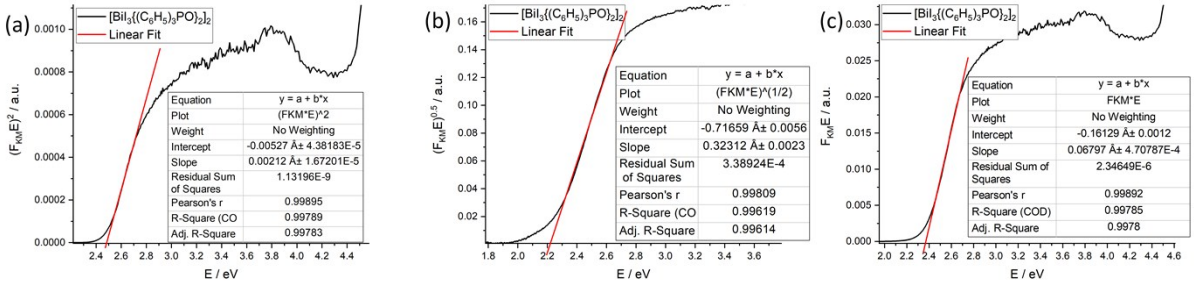

Figure S9. Tauc plots for $[BiI_3\{(C_6H_5)_3PO\}_2]_2$.

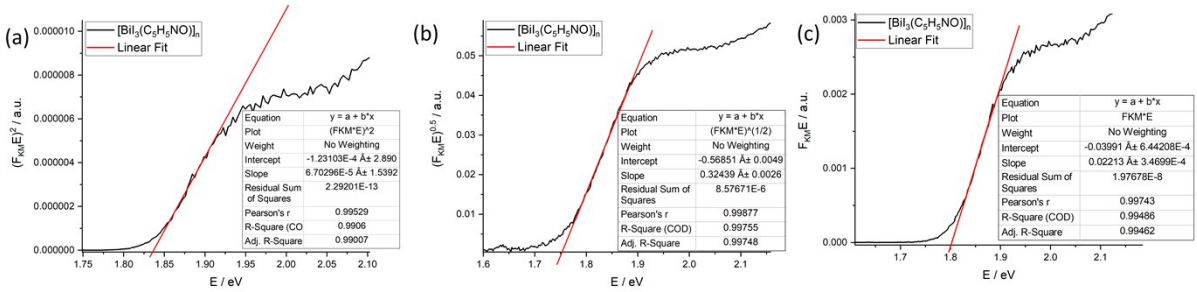

Figure S10. Tauc plots for $[BiI_3(C_5H_5NO)]_n$.

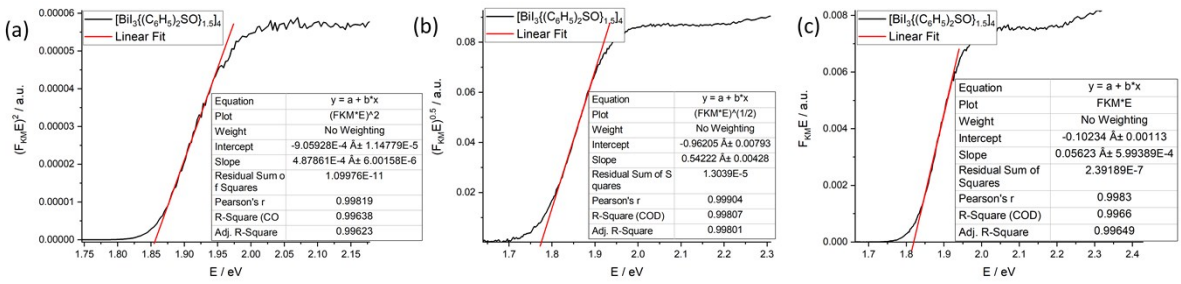

Figure S11. Tauc plots for $[BiI_3\{(C_6H_5)_2SO\}_{1.5}]$.

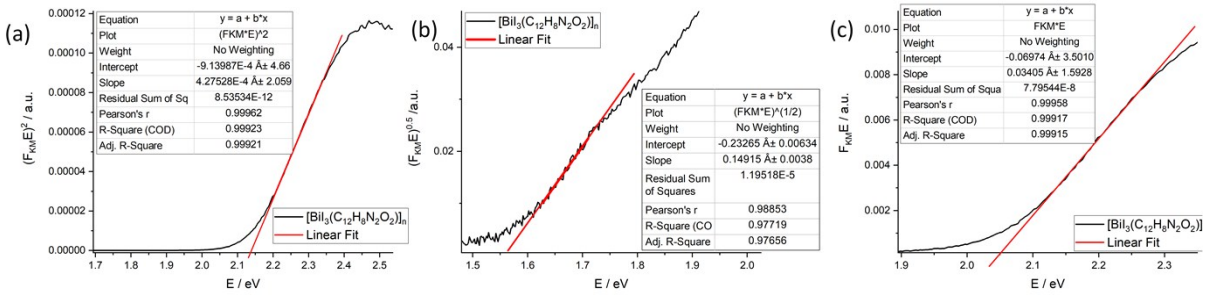

Figure S12. Tauc plots for $[BiI_3(C_{12}H_8N_2O_2)]_n$.

Table S2. Experimental and theoretical band gaps of studied compounds.

Compound	Experimental band gap / eV			Theoretical band gap / eV
	Direct	Indirect	Undefined	
BiI_3	–	**1.68**	–	indirect 1.18
$[BiI_3\{(C_6H_5)_3PO\}_2]_2$	2.49	2.22	**2.37**	Indirect 2.12
$[BiI_3\{(C_6H_5)_2SO\}_{1.5}]_4$	**1.86**	1.77	1.82	direct 1.87
$[BiI_3C_5H_5NO]_n$	1.84	**1.75**	1.8	indirect 1.81
$[BiI_3(C_{12}H_8N_2O_2)]_n$	2.13	**1.56**	2.05	indirect 1.33

Current-voltage characteristics

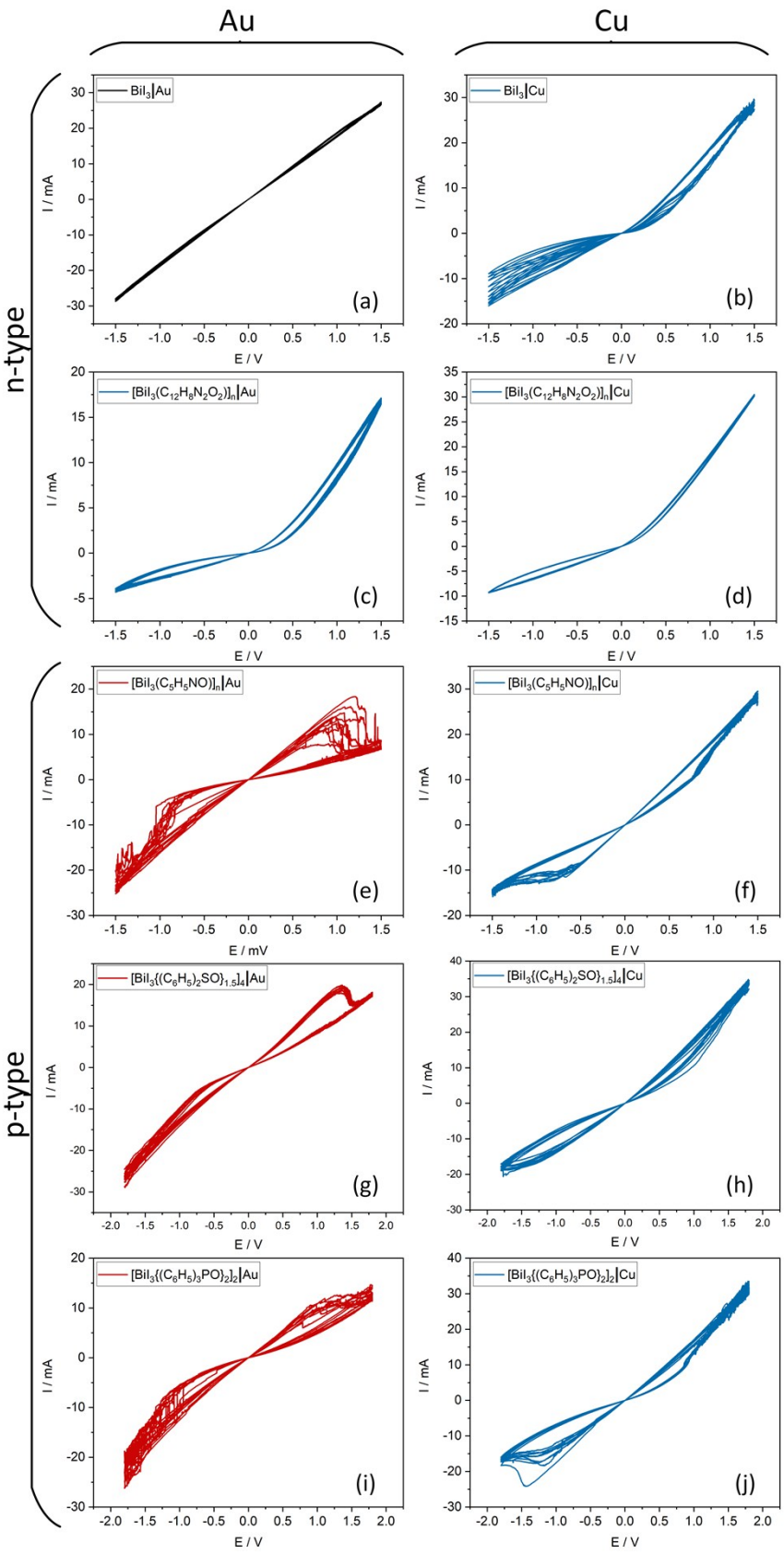

Figure S13. Current-voltage characteristics of BiI_3 memristors measured with Au (a) and Cu (b) as second electrode, $[BiI_3(C_{12}H_8N_2O_2)]_n$ memristors measured with Au (c) and Cu (d) as second electrode $[BiI_3(C_5H_5NO)]_n$ memristors measured with Au (e) and Cu (f) as second electrode, $[BiI_3\{(C_6H_5)_2SO\}_{1.5}]_4$ memristors measured with Au (g) and Cu (h) as second electrode, $[BiI_3\{(C_6H_5)_3PO\}]_2$ memristors measured with Au (i) and Cu (j) as second electrode. Ten scans with 100 S13

The stability of the states

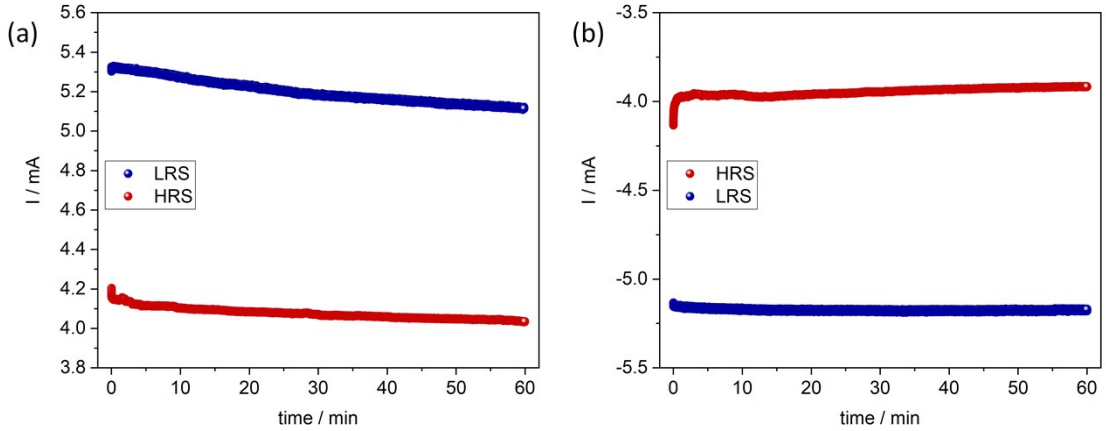

Figure S14. The persistence of the states measured at 0.3 V (a) and –0.3 V (b). The device (FTO/[BiI3{(C6H5)2SO}1.5]4/Au) was set to HRS with the 2.5 V (30 s) impulse and LRS with the –2.5 V (30 s) impulse.

Spike-timing dependent plasticity

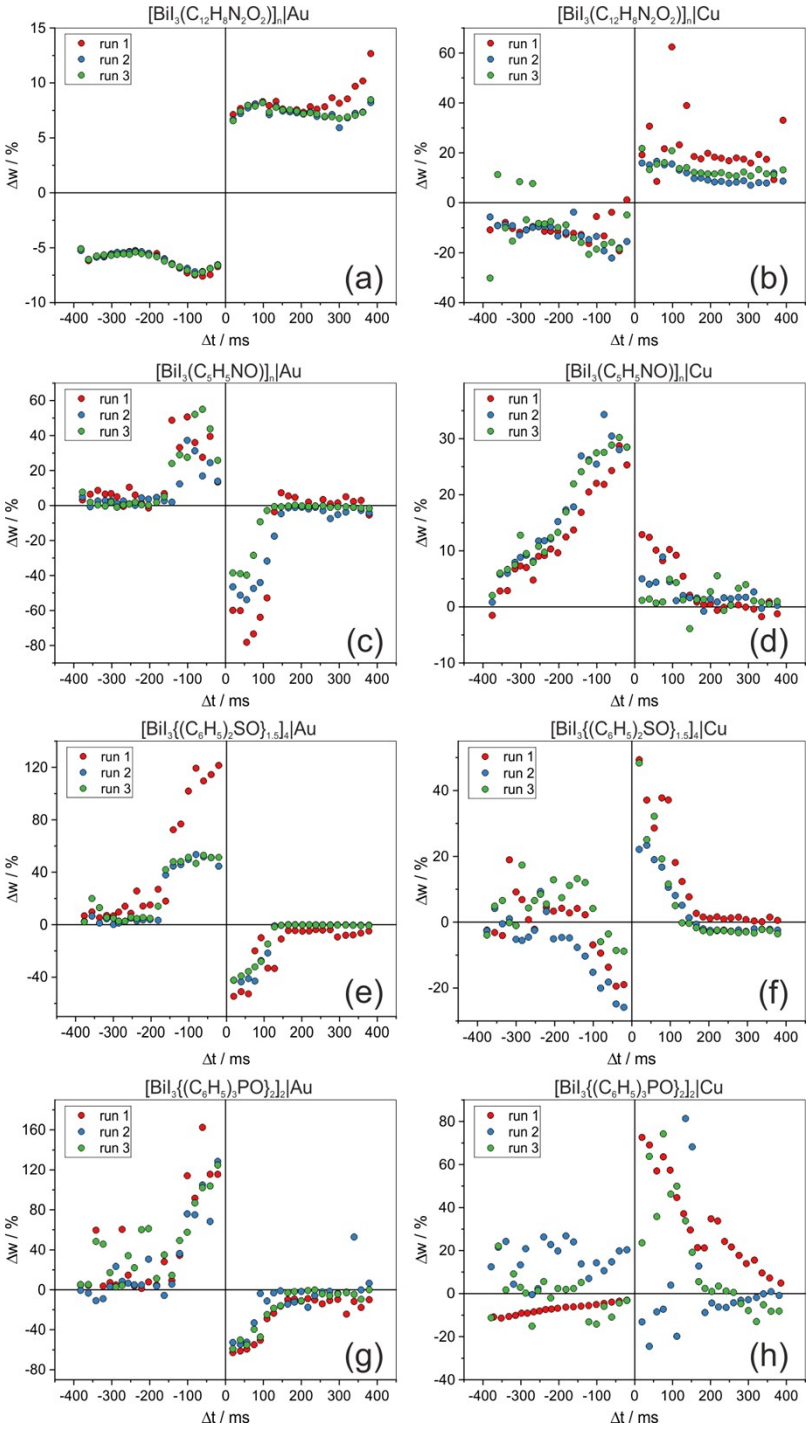

Figure S15. Spike-timing dependent plasticity (STDP) of the memristive materials measured of BiI_3 memristors measured with Au (left column) and Cu (right column) as second electrode, $[BiI_3(C_{12}H_8N_2O_2)]_n$ memristors measured with Au (a) and Cu (b) as second electrode $[BiI_3(C_5H_5NO)]_n$ memristors measured with Au (c) and Cu (d) as second electrode, $[BiI_3\{(C_6H_5)_2SO\}_{1.5}]_4$ memristors measured with Au (e) and Cu (f) as second electrode, $[BiI_3\{(C_6H_5)_3PO\}]_2$ memristors measured with Au (g) and Cu (h) as second electrode.

$[BiI_3(C_{12}H_8N_2O_2)]_n$

Due to narrow hysteresis loop in the I-V scan and rectifying character of the junction, $[BiI_3(C_{12}H_8N_2O_2)]_n$ shows no synaptic plasticity. Synaptic weight changes that can be seen both in Figure S14(a) and (b) are almost of constant value. This suggests that the applied voltage pattern caused only slight resistive switching, independent on the temporal interval between the spikes.

$[BiI_3(C_5H_5NO)]_n$

While $[BiI_3(C_5H_5NO)]_n|Au$ shows the expected antisymmetric anti-Hebbian behaviour, we have observed unipolar Hebbian learning rule with the Cu electrode. This phenomenon occurred due to instability of the current response to the applied voltage pattern or DC bias during the STDP measurement. The instability was monitored with I-V scans performed during the STDP measurements. The direction of resistive switching changes throughout the measurement.

$[BiI_3\{(C_6H_5)_2SO\}_{1.5}]_4$

This material was presented and described in the main text of the article (with the averaged Δw and error bars calculated as standard deviation). Here, we present the data collected during the 3 runs of the measurement.

$[BiI_3\{(C_6H_5)_3PO\}]_2$

Similarly to other materials measured with the Au electrode, $[BiI_3\{(C_6H_5)_3PO\}]_2$ also exhibits anti-Hebbian learning rule. However, data collected during the measurement with the Cu electrode is considerably scattered and differs among the measurement series. This material show instability in the I-V scans during the STDP measurement as well.